High temperature oxidation of carbides UHTC in air

Ludovic Charpentier, Marianne Balat-Pichelin, Diletta Sciti, Laura Silvestroni

HIGH TEMPERATURE OXIDATION OF CARBIDES UHTC IN AIR

Ludovic Charpentier[a], Marianne Balat-Pichelin[a] , Diletta Sciti [b], Laura Silvestroni [b]

[a] *PROMES-CNRS, 7 rue du Four Solaire, 66120 Font-Romeu Odeillo, France*
[b] *CNR-ISTEC, Institute of Science and Technology for Ceramics, 48018 Faenza, Italy*

Ludovic.Charpentier@promes.cnrs.fr; Marianne.Balat@promes.cnrs.fr; diletta.sciti@istec.cnr.it

Abstract. Ultra-High Temperature Ceramics having melting points above 3500 K and high thermal conductivities are envisaged to elaborate future receivers of concentration solar power plants. The high pressure and solar temperature reactor (*Réacteur Hautes Pression et Température Solaire*, REHPTS) at the focus of the Odeillo 5 kW solar furnace was used to investigate the oxidation of three carbides ($ZrC/MoSi_2$, $ZrC/TaSi_2$, $HfC/MoSi_2$) that could be candidate. The concentration of the additives ($TaSi_2$ or $MoSi_2$) was 20 v.% in each composition. Each sample was oxidized in static air (P = 87 kPa) during 20 minutes at 1800, 2000 and 2200 K. Experiments were filmed using a video camera and the gaseous phase was analyzed by mass spectrometry. Various characterizations have shown that the natures of the carbide and additive would affect the composition of the oxide layer and therefore the high-temperature behavior of the sample.

Keywords: UHTC, high temperature, oxidation, solar plants

INTRODUCTION

The efficiency of a concentration solar power plant strongly relies on the high temperature behavior of the solar receiver. Silicon carbide (SiC) begins to be one ceramic material used to produce various geometries for solar absorbers [1, 2], but the degradation of the material becomes too important above 1700 K because of the formation of bubbles and the production of gaseous SiO and CO which implies a severe mass loss of the material. Therefore a SiC receiver cannot be heated at a temperature so high that the air coolant can issue it above 1100 K. Consequently, an extra source of fossil energy (or biomass) has to be added after the receiver in order to end up the heating of pressurized air up to more than 1300 K and therefore insure a sufficient efficiency of the energy conversion to make the technology financially viable [3].

We have therefore studied the oxidation behavior of new ultra-high temperature ceramics (UHTC) having good mechanical properties even above 2300 K, in order to identify which would be the best candidates to elaborate new high temperature solar receivers. Among potential materials for such application, zirconium carbide (ZrC) presents a high melting point (3500 K) and interesting mechanical properties, especially its hardness around 27 GPa, making of it one of the hardest materials among UHTC [4]. The main limitation for high temperature applications is the oxidation kinetics: zirconia (ZrO_2) is non protective and ZrC continuously oxidizes according to a linear kinetic [5]. Incorporation of silicon was found to enable the formation of mixed oxide layer such as zircon ($ZrO_2 \cdot SiO_2$), which was shown to improve the resistance to oxidation [6]. Sarin *et al.*[7] also recently reported the thickness of the oxide layer formed on ZrB_2/SiC composite materials during oxidation in air around 1500 K decreased when the amount of SiC in the initial material increased from 0 till 50 v.%.

We decided to focus on two carbides with disilicide additives as several routes were recently developed at ISTEC-CNR to elaborate such materials by pressureless sintering or hot pressing [8-11]. The first material we deeply investigated was ZrC with $MoSi_2$ additive [12]. We have decided to compare the behavior of $ZrC/MoSi_2$ with the behaviors of $HfC/MoSi_2$ or $ZrC/TaSi_2$, changing either the carbide or the additive.

EXPERIMENTAL PROCEDURE

The reactor we used to perform high temperature oxidation is the REHPTS (*Réacteur Hautes Température et Pression Solaire*, High Temperature and Pressure Reactor), at the focus of the Odeillo 5 kW solar furnace, shown in figure 1.

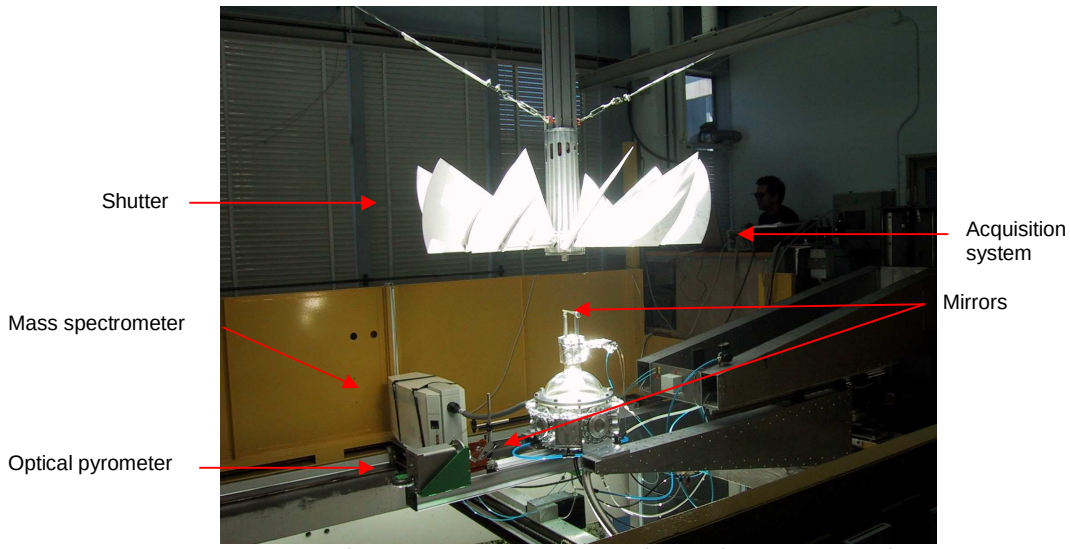

FIGURE 1. View of the REHPTS reactor at the focus of the 5kW solar furnace.

A flat mirror (heliostat) whose position is servo-controlled to the apparent movement of the sun reflects the incident solar flux to a concentrator with facetted mirrors. A shutter enables to control the fraction of the concentrated solar flux delivered to the sample placed inside the reactor and therefore its surface temperature. This set-up is placed so that the sample is 25 mm above the focus of the solar furnace, thus elevated temperatures on materials may be obtained at very fast rate (up to 100 K s^{-1}) on a homogeneous 10 mm diameter area. Two mirrors enable a monochromatic (5 µm) optical pyrometer (Ircon, Modline Plus) to measure the surface temperature of the sample through a fluorine window. The pyrometer with all the parts present on the optical path was calibrated on a black body. The accuracy of the temperature measurements is going from 1400 ± 15 K to 2100 ± 22 K. A mass spectrometer (Pfeiffer Omnistar) enables *in situ* gas phase analysis.

Materials were elaborated by ISTEC-CNR in Faenza, Italy. ZrC/20 v.% $MoSi_2$ (final density: 95%, 6.2 g.cm^{-3}) and HfC/20 v.% $MoSi_2$ (f. d.: 97%, 11.1 g.cm^{-3}) were produced by pressureless sintering at 2220 K during 90 min. ZrC/20 v.% $TaSi_2$ (f. d.: 99%, 7.1 g.cm^{-3}) was sintered by Hot Pressing under 30 MPa loading at 1970 K during 6 min. The samples were shaped into 25mm-diameter and 2mm-thickness discs cut using Electrical Discharge Machining (EDM). This technique consists in cutting the material thanks to rapid discharges between two electrodes, so that the material locally reaches its melting temperature. This might allow the formation of zirconia at the surface during cutting. Thermodynamic calculations were performed using the GEMINI [13] software in order to compare the stable products due to the oxidation of both ceramics in air.

The oxidations were performed in static air. Due to the altitude of the laboratory, the total atmospheric pressure is around 87 kPa and the oxygen partial pressure pO_2 is 17 kPa. The surface temperature of the samples was maintained at a constant plateau during 20 min. and a video camera was used to follow *in situ* the oxidation process. Mass spectrometry enables to identify the gaseous products. As explained further in the results from thermodynamic calculation, CO is expected to be the main gaseous product during oxidation, but its molar weight is the same as N_2 one (m/e = 28), so it is impossible to separate the contribution of CO from the one of preponderant N_2. Therefore we mainly follow the signal corresponding to m/e = 44, corresponding both to CO_2 and gaseous SiO.

The samples were weighted before and after oxidation in order to access the mass variation (converted to a mass variation rate expressed in mg cm^{-2} min^{-1}). Some surfaces have been analyzed after oxidation using XRD and SEM with EDS.

RESULTS AND DISCUSSION

Thermodynamic calculations

Figures 2 to 4 present the amount in moles of solid phases and the molar fraction of main gaseous products (the gaseous phase being completed with N_2, not plotted on the graph) according to the temperature at the thermodynamic equilibrium with the following initial conditions:

- 8 moles of carbide (ZrC or HfC)
- 2 moles of additive ($MoSi_2$ or $TaSi_2$)
- 10 moles of air (8 moles N_2, 2 moles O_2)
- Total pressure: 10^5 Pa

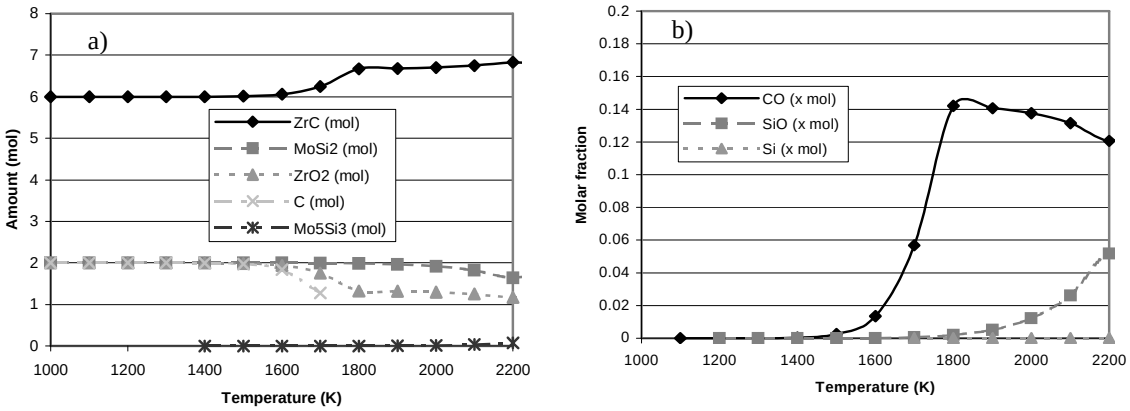

FIGURE 2. Amount of solid phases (a) and molar fraction of main gaseous products (b) at thermodynamic equilibrium according to temperature, calculated using GEMINI software. Initial conditions: 8 moles ZrC, 2 moles $MoSi_2$, 8 moles N_2, 2 moles O_2, P = 10^5 Pa, $pO_2 = 2.10^4$ Pa.

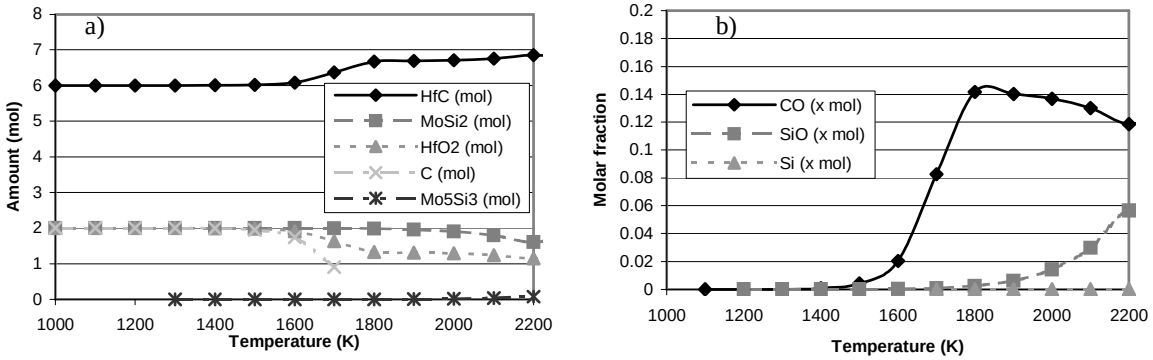

FIGURE 3. Amount of solid phases (a) and molar fraction of main gaseous products (b) at thermodynamic equilibrium according to temperature, calculated using GEMINI software. Initial conditions: 8 moles HfC, 2 moles $MoSi_2$, 8 moles N_2, 2 moles O_2, P = 10^5 Pa, $pO_2 = 2.10^4$ Pa.

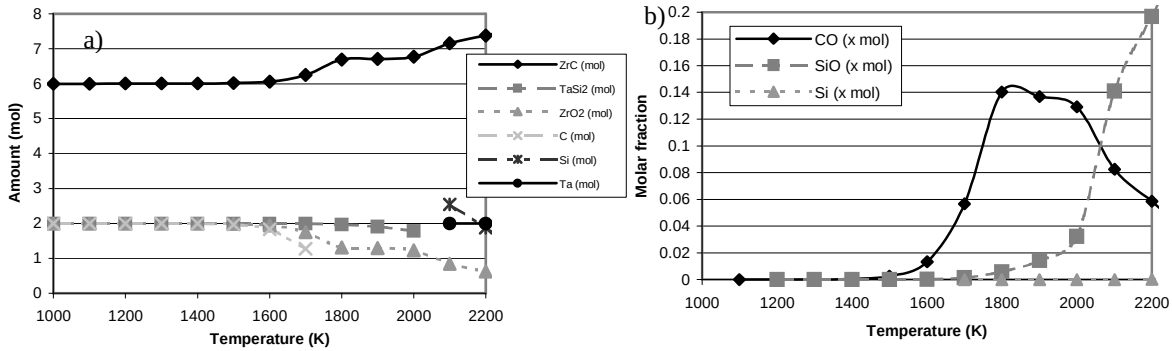

FIGURE 4. Amount of solid phases (a) and molar fraction of main gaseous products (b) at thermodynamic equilibrium according to temperature, calculated using GEMINI software. Initial conditions: 8 moles ZrC, 2 moles $TaSi_2$, 8 moles N_2, 2 moles O_2, P = 10^5 Pa, pO_2 = 2.10^4 Pa.

Comparing figures 2 and 3 shows hardly no difference between ZrC/$MoSi_2$ and HfC/$MoSi_2$, except obviously that the main solid oxide is ZrO_2 in figure 2 (a), HfO_2 in figure 3 (a). The main gaseous oxides are CO and SiO. The molar fraction of this latest oxide increases with the temperature from 1800 to 2000 K. Comparing figures 2 and 4 shows that $TaSi_2$ is less stable at high temperature than $MoSi_2$: in figure 4 (a), $TaSi_2$ decomposes itself into Ta and Si beyond 2100 K, whereas in figure 2 (a), $MoSi_2$ stays present up to 2200 K. As a consequence of this weaker stability, the molar fraction of SiO produced in figure 4 (b) is far higher above 2000 K than in figure 2 (b).

In situ analyses

Video images

Figures 5 to 7 present video captions of the various materials after 15 minutes of oxidation tests in air at 1800, 2000 and 2200 K respectively.

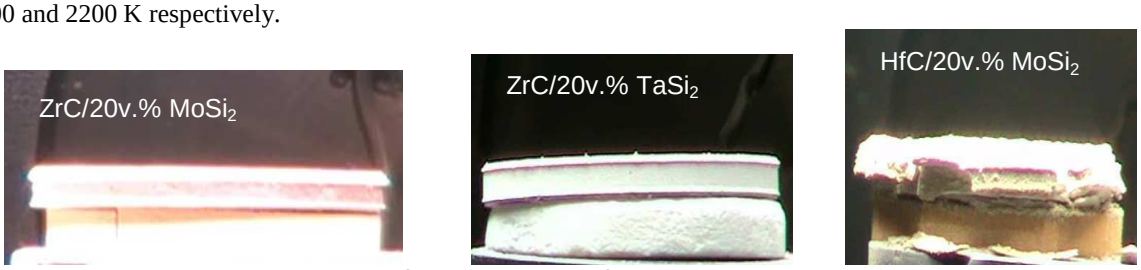

FIGURE 5. Video captions of the three UHTC after 15 min. oxidation tests in air at 1800 K

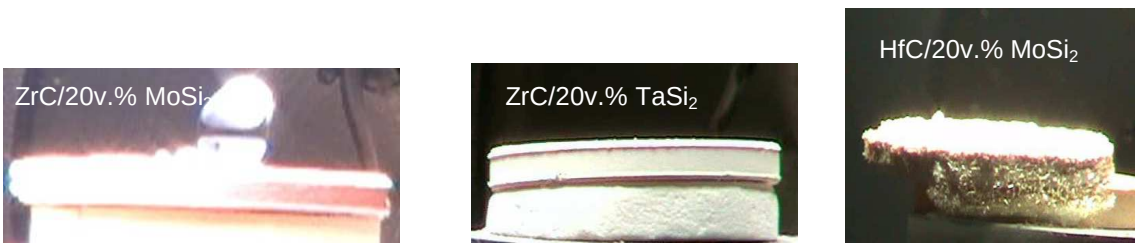

FIGURE 6. Video captions of the three UHTC after 15 minutes of oxidation tests in air at 2000 K

FIGURE 7. Video captions of the three UHTC after 15 minutes of oxidation tests in air at 2200 K

We can observe in figure 5 that at 1800 K, the oxide layer that forms on ZrC materials looks adherent to the carbide, whereas the oxide layer that forms on HfC is breaking into several fragments. This can be explained by the thermal expansion: HfC has a higher thermal expansion coefficient than HfO_2 ($6.6x10^{-6}$ mm^{-1} K^{-1} vs. $5.6x10^{-6}$ mm^{-1} K^{-1}), so the oxide layer can break due to the expansion of the carbide. On the other side, ZrC has a lower coefficient than ZrO_2 ($6.7x10^{-6}$ mm^{-1} K^{-1} vs. 10^{-5} mm^{-1} K^{-1}), so the oxide dilates more than the carbide, which can explain why the oxide layer covers a larger area over the carbide.

In figure 6, we can observe a bubble on the ZrC/20v. % $MoSi_2$. This bubble may be due to the formation of silica that is liquid at 2000 K, and it can blow due to the production of gaseous CO or SiO, which are expected products from the thermodynamical calculations. There is still a fragile oxide that breaks on the HfC material, that has slightly moved from the support due to the release of gaseous products. ZrC/20 v.% $TaSi_2$ seems to be the less damaged. This observation is confirmed at 2200 K (figure 7): whereas ZrC/20v. % $MoSi_2$ and HfC/20v.% $MoSi_2$ support an important boiling, the oxide on ZrC/20 v.% $TaSi_2$ supports a less important deformation due to the presence of tantalum.

Mass spectrometry

Figure 8 is presenting the evolution of the CO_2 and SiO concentration determined using mass spectrometry. We can observe that at 1800 and 2000 K the HfC/ 20%v. $MoSi_2$ is the material that releases the highest amount of gaseous products during oxidation. This can be due to the fact its oxide layer breaks as seen in figure 5 and 6 and enables the gases to escape from the oxide/carbide interface. Nevertheless the production of gases decreases after 10 minutes, probably due to the formation of a protective oxide layer preventing the release of gaseous products. Equivalent amount of gases is detected during the oxidation of ZrC/$MoSi_2$ and ZrC/$TaSi_2$ materials at 1800 K and during the 600 first seconds of oxidation at 2000 K. During the second half of the oxidation at 2000 K, there are more gases released by ZrC/$TaSi_2$ than by ZrC/$MoSi_2$. We can give a first explanation from the results of thermodynamic calculations (figures 2 and 4): additive is less stable under oxidizing atmospheres than $MoSi_2$, and therefore more SiO is produced. A second explanation comes from the video observations: liquid oxide blows at the surface of ZrC/$MoSi_2$ and can therefore prevent gaseous products from being released. Presence of tantalum seems to limit the presence of big bubbles of liquid oxide, therefore gaseous products may faster escape through fissures and the bursting of smaller bubbles. Both hypotheses could also explain why ZrC/$TaSi_2$ releases more CO_2 and SiO at 2200 K than the two other materials. We observe that the higher is the temperature, the most important is the amount of gaseous products released on both ZrC materials, in agreement with the thermodynamic calculations. For HfC/$MoSi_2$ the production of gases increases from 1800 to 2000 K, then decreases from 2000 to 2200 K. The apparition of liquid oxide that blows and may fill the fissures in the oxide layer could explain why less gaseous products can be released at 2200 K than at 2000 K.

Mass variations

Table 1 shows the global mass variations for each material. The higher is the temperature, the faster is the oxide growth. The mass variation of the HfC/$MoSi_2$ is much lower (and negative at 1800 K) than the one of the ZrC materials, which can be explained by the important breaking and removal of the oxide layer on HfC during the experiments. The nature of the additive in the ZrC materials has hardly influence at 1800 K. At higher temperature, the mass variation is more important when $TaSi_2$ is used. Tantalum seems therefore to play a significant role in the oxide formation, post-experiment analyses should enable us to accede the composition of the oxide layers and to understand this influence.

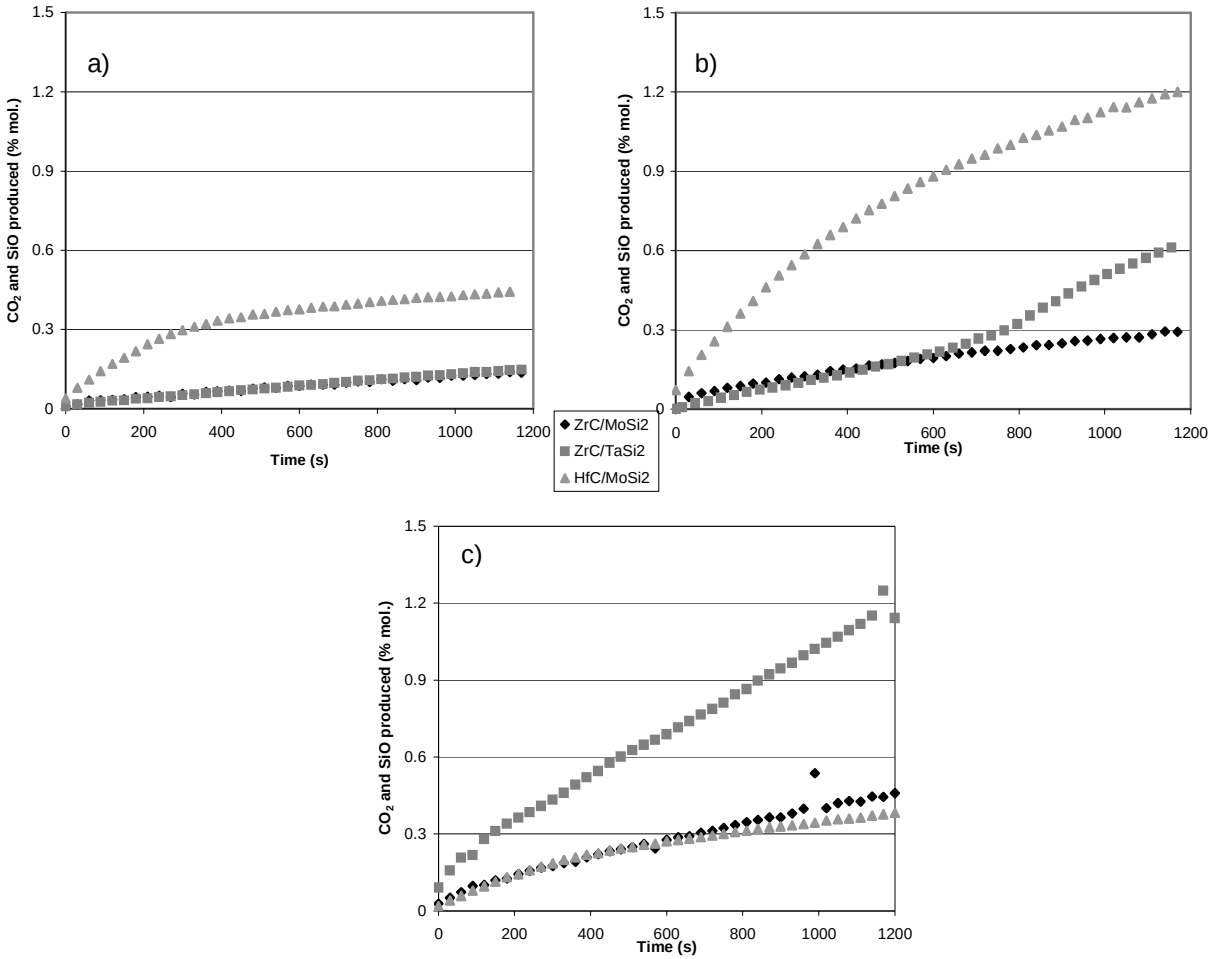

FIGURE 8. Measurement of the concentration at m/e = 44 (SiO and CO_2 produced) at a) 1800 K b) 2000 K c) 2200 K during the oxidation of the UHTC materials.

TABLE 1. Average mass variation rates for each sample according to the temperature

Temperature (K)	$ZrC/MoSi_2$ ($mg.cm^{-2}.min^{-1}$)	$HfC/MoSi_2$ ($mg.cm^{-2}.min^{-1}$)	$ZrC/TaSi_2$ ($mg.cm^{-2}.min^{-1}$)
1800	1.28	- 0.20	1.20
2000	1.72	0.61	2.37
2200	2.23	1.42	3.86

Post-experimental characterizations

X-Ray Diffraction

Figure 9 is presenting the XRD patterns for samples of each composition before and after 20 minutes oxidation in air. The reference patterns we used for the indexation are: 19-1487 (cubic ZrC), 80-0544 (tetragonal $MoSi_2$), 65-8750 (cubic HfC), 83-0944 (monoclinic ZrO_2), 65-1142 (monoclinic HfO_2), 77-1759 (tetragonal $HfSiO_4$), 42-0060 (orthorhombic $TaZr_{2.75}O_8$). Figure 9 (a) shows that the only crystalline phase which forms on ZrC/20 v.% $MoSi_2$ is monoclinic zirconia. In figure 9 (b), we cannot identify on the reference sample any pattern of the $TaSi_2$ additive, but we observe the main crystalline phase is not zirconia (whose we can nevertheless still identify its two main peaks), but orthorhombic tantalum-zirconium oxide $TaZr_{2.75}O_8$. This difference in the composition of the final oxide

probably explains why ZrC/20 v.% $TaSi_2$ gains more mass (table 1) and its oxide layer supports less deformation (figures 6 and 7) than ZrC/20 v.% $MoSi_2$ above 1800 K.

We observe in figure 9 (c) that the main crystalline phase that has grown on HfC/20v.% $MoSi_2$ is monoclinic hafnia, but the presence of tetragonal hafnium-silicon oxide $HfSiO_4$ was also evidenced.

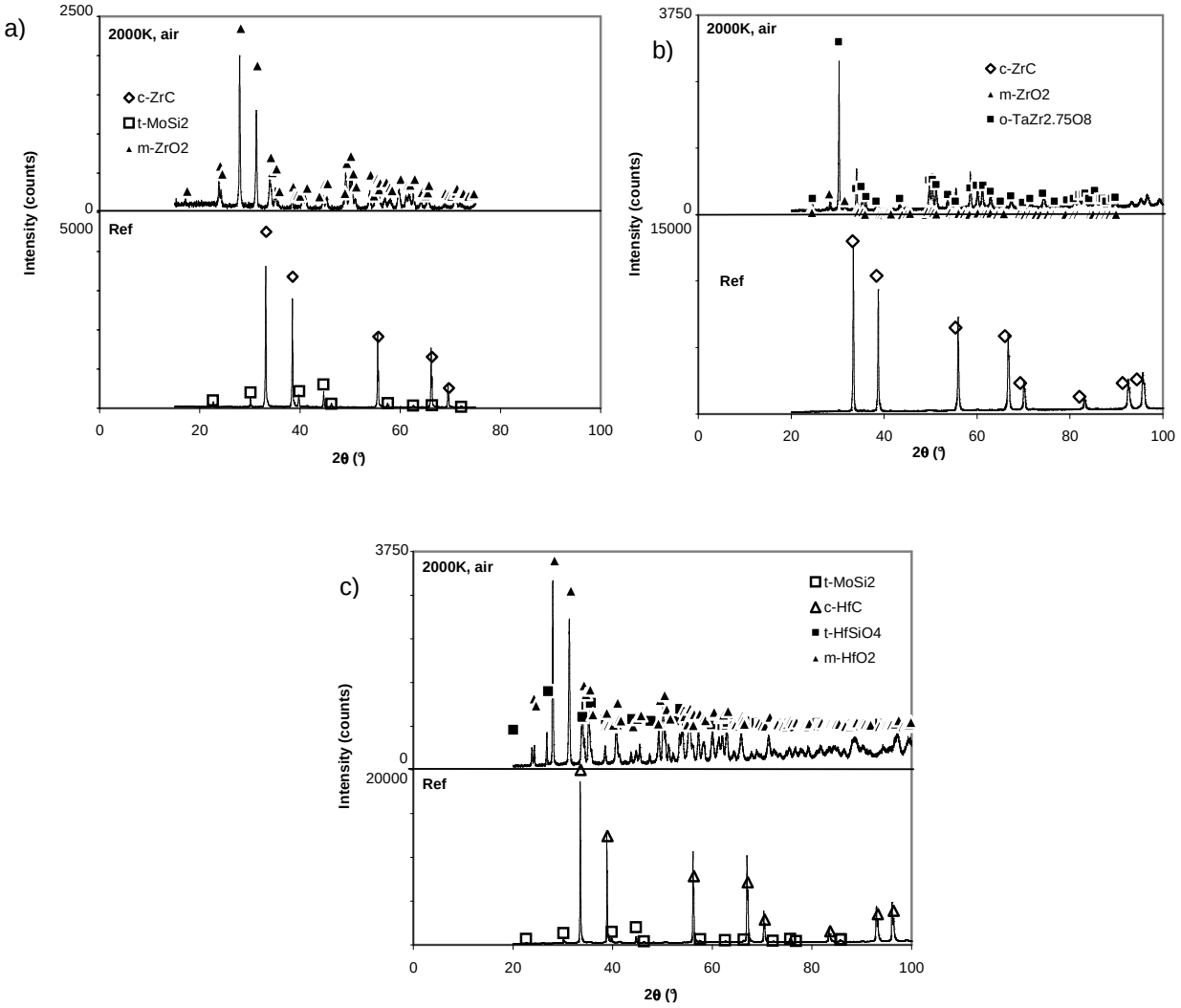

FIGURE 9. XRD patterns of materials, reference and oxidized during 20 min. in air at 2000K. a) ZrC/20 v.% $MoSi_2$ b) ZrC/20 v.% $TaSi_2$ c) HfC/20 v.% $MoSi_2$

Cross-section SEM and EDS

Figures 10 to 12 present cross-section SEM images of the oxide layers (phases were identified using EDS) on ZrC/$MoSi_2$, ZrC/$TaSi_2$ oxidized in air at 2000 K.

The total modified area on ZrC/$MoSi_2$ is 435µm-thick in all and can be divided into 5 different layers (figure 10 (a)). Layer 1 is 30 µm-thick silica, probably amorphous as we could not detect any silica phases through XRD (figure 9 (a)). Layer 2 is 150µm-thick and its composition is brain-like ZrO_2 (mainly monoclinic from XRD) surrounded by darker SiO_2 as shown on figure 10 (b). Layer 3 consists of 85 µm-thick porous and brittle ZrO_2. Layer 4, 80-µm thick, involves dense ZrC grains surrounded by granulous Zr-C-O, $MoSi_2$ and Mo_5Si_3 surrounded by thin SiO_2 layer. Finally, layer 5, 90 µm-thick, is composed with the same phases as in layer 4, plus some SiC. ZrO_2 forms from the oxidation of the carbide and our observations seem coherent with the mechanism proposed by

Shimada [14]: an intermediary oxycarbide forms close to the interface with ZrC, then further completely oxidized into ZrO_2. SiO_2 forms due to the oxidation of the additive, together with the production of Mo_5Si_3, then moves toward the top surface of the oxide. SiC grains in layer 5 show that some more complex reactions, involving both the carbide and additive may occur close to the interface.

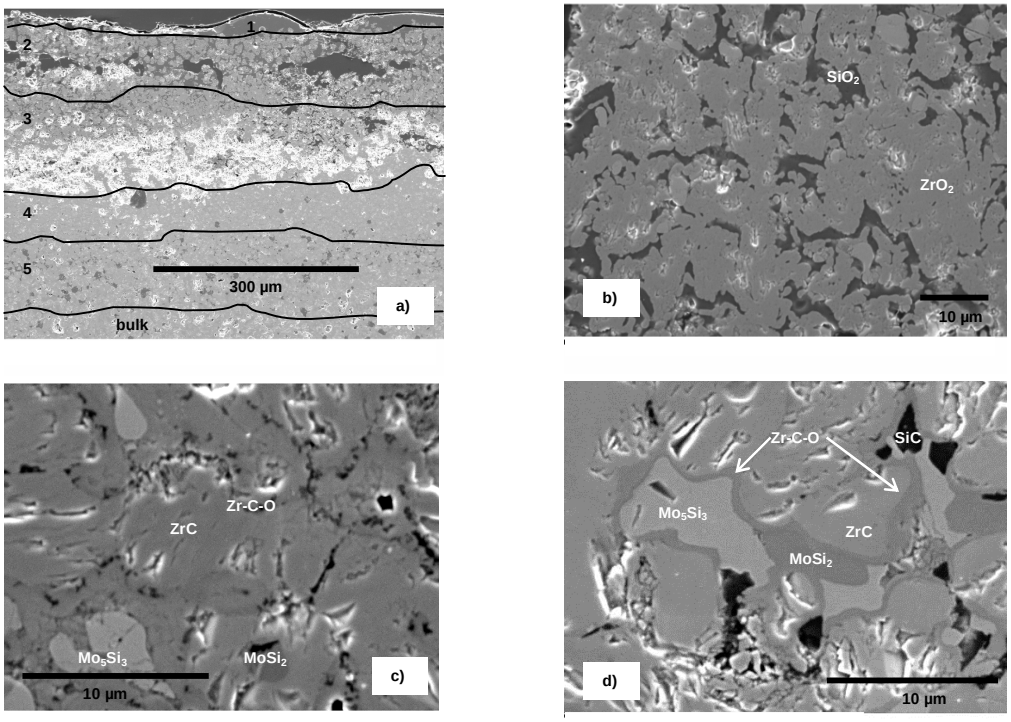

FIGURE 10. Cross-section SEM images of a ZrC/20 v.% $MoSi_2$ sample after 20 min. oxidation in air at 2000 K. a) Global cross-section, b) zoom on modified layer 2, c) zoom on modified layer 4, d) zoom on modified layer 5.

The modified area on ZrC/$TaSi_2$ (figure 11 (a)) has nearly the same total thickness (430 µm) as for ZrC/$MoSi_2$ and can be divided into only three layers. The first layer (figure 11 (b)), 110-µm thick, mainly consists of $TaZr_{2.75}O_8$, with some inclusions of Si-C-O phases. In the 80µm-thick second layer (figure 11 (c)), $TaZr_{2.75}O_8$ is still mainly found, but the secondary phase is SiC. Finally, the 240 µm-thick third layer is a complex mixture of (Zr,Ta)Si_2 (white), (Zr, Ta)-C-O (grey), and SiC (black) phases. Oxidation of this material looks more complex: both carbide and additive reacts with oxygen to form mixed oxide (the oxycarbide and disilicide phases observed close to the interfaces are probably intermediate compounds) and SiC, that has partially oxidized close to the surface. Some gaseous SiO may also be produced, which could explain the mass spectrometry measurement in figure 8 (b). According to Bhattacharya *et al.* [15] who computed a recent phase diagram for the ZrO_2 – Ta_2O_5 system, zirconium – tantalum – oxygen solution melts from 2100 K, which could explain why no deformation is observed at 2000 K in figure 6 whereas silica formed on ZrC/$MoSi_2$ material may melt and blow due to gaseous release.

Only one 100µm-thick layer was remaining at the surface of HfC/$MoSi_2$ (figure 12 (a)). Its composition involves HfO_2, SiO_2, Mo_5Si_3 and $HfSiO_4$ (figure 12 (b)). This latest compound melts incongruently at 2020 K [16]. So the presence of this mixed oxide may explain why little boiling is observed at 2000 K on the surface of HfC/$MoSi_2$ compared with ZrC/$MoSi_2$. We can notice an important porosity through the remaining oxide, favouring the gaseous release.

The calculations could not predict the stability of $HfSiO_4$ and $TaZr_{2.75}O_8$ because the thermodynamic data of both mixed oxides are not well-known and therefore they could not be included in the calculations. Moreover, the calculations considered only the thermodynamic equilibrium and did not take into consideration kinetic control or the energy required to create interfaces, that is the reason why the solid compounds observed are slightly different than the ones predicted by the thermodynamic calculations.

CONCLUSIONS

Oxidation of ZrC/20 v. % $MoSi_2$ occurs with important boiling above 2000 K due to the production of molten silica and gaseous products (SiO, CO). Changing either the carbide (HfC/20 v.% $MoSi_2$) or the additive (ZrC/20 v.% $TaSi_2$) appears to reduce the deformation of the materials at 2000 K through the production of mixed oxides ($HfSiO_4$ or $TaZr_{2.75}O_8$) with higher melting points than silica. Nevertheless, HfC produces a very fragile oxide that breaks during oxidation, producing solid particles and therefore HfC does not seem accurate for the conception of solar receivers at temperature lower than 2000 K. One drawback of tantalum incorporation is that liquid $TaZr_{2.75}O_8$ may flow out of the sample at 2200 K [16]. These removals have to be avoided as they would favour continuous oxidation. In our future works, we will develop tests on ZrC/SiC materials to check the influence of another additive as these materials under development seem promising [17, 18]. Another solution to get high temperature resistive materials could be to use two additive (ZrC/$MoSi_2$/$TaSi_2$ or ZrC/SiC/$TaSi_2$), with a smaller amount of tantalum as recommended by Opila *et al*. [16].

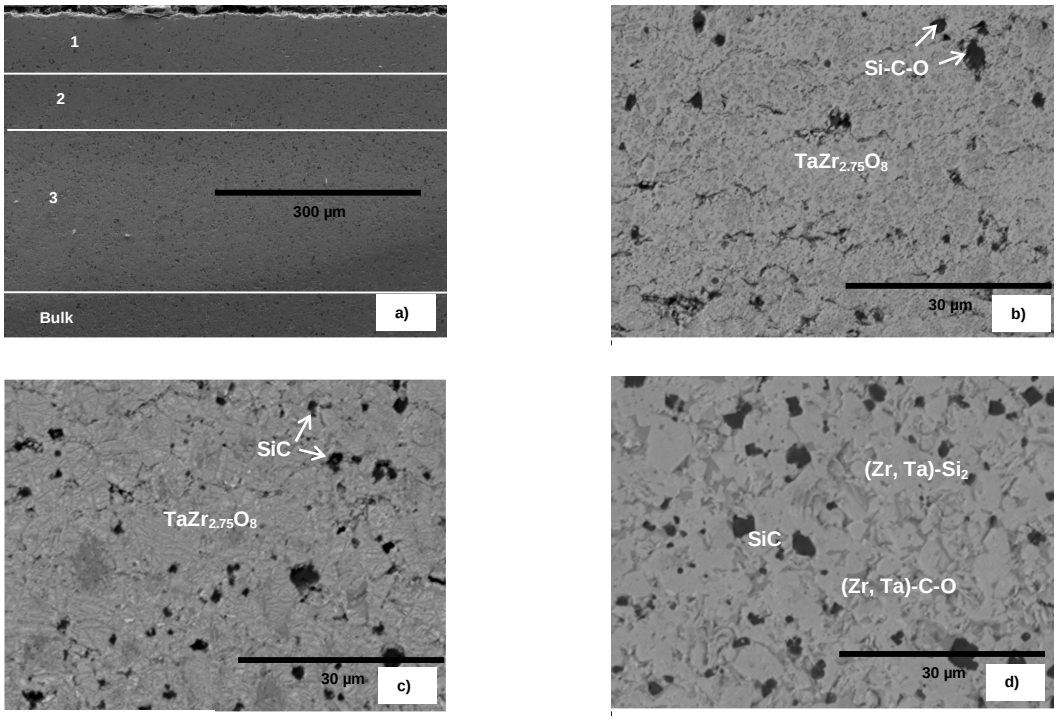

FIGURE 11. Cross-section SEM images of a ZrC/20 v.% $TaSi_2$ sample after 20 min. oxidation in air at 2000 K. a) Global cross-section, b) zoom on modified layer 1, c) zoom on modified layer 2, d) zoom on modified layer 3.

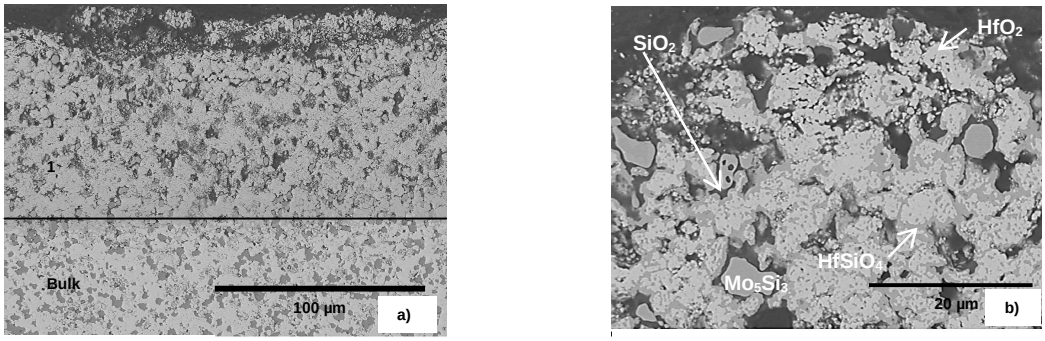

FIGURE 12. Cross-section SEM images of a HfC/20 v.% $MoSi_2$ sample after 20 min. oxidation in air at 2000 K. a) Global cross-section, b) zoom on modified layer 1

REFERENCES

1. C. C. Agrafiotis, I. Mavroidis, A. G. Konstandopoulos, B. Hoffschmidt, P. Stobbe, M. Romero and V. Fernandez-Quero *Solar Energy Materials and Solar Cells*, **91**, 474 (2007).
2. Z. Wu, C. Caliot, F. Bai, G. Flamant, Z. Wang, J. Zhang and C. Tian *Applied. Energy*, **87**, 504 (2010).
3. P. Garcia, A. Ferrière, G. Flamant, P. Costerg, R. Soler and B. Gagnepain *Journal of Solar Energy Engineering*, **130**, 014502 (2008).
4. M. J. Gasch, D. T. Ellerby and S. M. Johnson, in: *Handbook of Ceramic Composites, Part II*, 2005, pp. 197-224.
5. S. Shimada, *Journal of the American Ceramic Society*, **73**, 2804 (1990).
6. D. Gao, Y. Zhang, J. Fu, C. Xu, Y. Song and X. Shi, *Corrosion Science*, **52**, 3297 (2010).
7. P. Sarin, P. E. Driemeyer, R. P. Haggerty, D. K. Kim, J. L. Bell, Z. D. Apostolov and W. M. Kriven, *Journal of the European Ceramic Society*, **30**, 2375 (2010).
8. D. Sciti, S. Guicciardi and M. Nygren, *Scripta Materialia*, **59**, 638 (2008).
9. L. Silvestroni, D. Sciti, J. Kling, S. Lauterbach and H. J. Kleebe, *Journal of the American Ceramic Society*, **92**, 1574 (2009).
10. D. Sciti, L. Silvestroni and A. Bellosi, *Journal of the American Ceramic Society*, **89**, 2668 (2006)
11. L. Silvestroni and D. Sciti, *Journal of Material Research*, **23**, 1882 (2008).
12. B. Pierrat, M. Balat-Pichelin, L. Silvestroni and D. Sciti, *Solar Energy Materials and Solar Cells*, **95**, 2228 (2011).
13. Thermodata, Saint Martin d'Hères, France.
14. S. Shimada, *Solid State Ionics*, **141-142**, 99 (2001).
15. A. K. Bhattacharya, V. Shklover, W. Steurer, G. Witz, H. P. Bossmann and O. Fabrichnaya, *Journal of the European Ceramic Society*, **31**, 249 (2011).
16. E. Opila, S. Levine and J. Lorincz, *Journal of Materials Science*, **39**, 5969 (2004).
17. Z. Liyou, J. Dechang, D. Xiaoming, Y. Zhihua and Z. Yu, *International Journal of Refractory Metals and Hard Materials*, **29**, 516 (2011)
18. D. Pizon, R. Lucas, S. Foucaud and A. Maître, *Advanced Engineering Materials*, **13**, 599 (2011)